Ideal shear strain of metals and ceramics

Shigenobu Ogata,[1,2,3] Ju Li,[4] Naoto Hirosaki,[5] Yoji Shibutani,[2,3] and Sidney Yip[1,6,*]
[1]*Department of Nuclear Engineering, Massachusetts Institute of Technology, Cambridge, Massachusetts 02139, USA*
[2]*Handai Frontier Research Center, Osaka University, Osaka 565-0871, Japan*
[3]*Department of Mechanical Engineering and Systems, Osaka University, Osaka 565-0871, Japan*
[4]*Department of Materials Science and Engineering, Ohio State University, Columbus, Ohio 43210, USA*
[5]*Advanced Materials Laboratory, National Institute for Materials Science, Ibaraki, 305-0044, Japan*
[6]*Department of Materials Science and Engineering, Massachusetts Institute of Technology, Cambridge, Massachusetts 02139, USA*
(Received 29 March 2004; revised manuscript received 18 May 2004; published 15 September 2004)

Using density functional theory we analyze the stress-strain responses of 22 simple metals and ceramics to determine the maximum shear strain a homogeneous crystal can withstand, a property for which we suggest the name shearability. A shearability gap is found between metals and covalent ceramics. Shearability of metals further correlates with the degree of valence charge localization and directional bonding. Depending on the deformation constraints, ionic solids may possess even larger shearability than covalent solids. The Frenkel model of ideal shear strength works well for both metals and ceramics when shearability is used in the scaling.

DOI: 10.1103/PhysRevB.70.104104 PACS number(s): 62.20.−x, 81.40.Jj

The ductility of solids is controlled by the energy needed to break a bond by shear compared to that by tension.[1–7] It is characteristic of ceramics to have a larger ratio of shear to bulk moduli; however, little is known about the range of shear deformation in solids with different types of bonding. The maximum shear and tensile distortions that chemical bonding can withstand are particularly important for defects, e.g., dislocation cores and crack tips.[6,7] A first step toward better understanding begins with two aspects of affine deformation of perfect crystals. One is the elastic constant describing the linear response of the lattice to small strain, and the other is a fundamental characterization of the large-strain nonlinear response.[8–11] While use of the former in scaling relations is almost universal in defect mechanics, the question of whether the latter also factors into microstructure-controlling quantities such as the intrinsic stacking fault energy has been examined only recently.[12] Here we apply density functional theory (DFT) to compute the shearability and tensibility of simple metals and ceramics, defined by the maximum shear and tensile strains at which a perfect crystal under affine deformation becomes unstable, to bring out the fundamental connection between critical mechanical response of a solid and the underlying electronic structure such as redistribution of valence charge density. To be precise, we define shearability as $s_m \equiv \arg\max \sigma(s)$, where $\sigma(s)$ is the resolved shear stress and s is the engineering shear strain in a specified slip system. Similarly, tensibility is taken to be $t_m \equiv \arg\max -P((1+t)V_0)$, where $P(V)$ is the pressure-volume relation and V_0 is the equilibrium volume, $P(V_0)=0$.

We have studied the following metals and ceramics using the Vienna *Ab-Initio* Simulation Package[13]: FCC Ag, Cu, Au, ferromagnetic (FM) and paramagnetic (NM) Ni, Al; BCC W, Mo, Fe(FM); HCP Mg, Ti, Zn; $L1_0$ TiAl, $D0_{19}$ Ti_3Al; diamond cubic C, Si; β−SiC, $\alpha-,\beta-Si_3N_4$; B1 NaCl, MgO, KBr, CaO. The exchange-correlation density functionals adopted are Perdew-Wang generalized gradient approximation (GGA) for metals except Au and Ag, and Ceperley-Alder local density approximation (LDA) for the others. Ultrasoft (US) pseudopotential is used in most cases, but for difficult systems we switch to the projector augmented-wave (PAW) method.[14] Brillouin zone (BZ) $\boldsymbol{k}$-point sampling is performed using the Monkhorst-Pack algorithm. For metals, BZ integration follows the Methfessel-Paxton scheme [15] with the smearing width chosen so the "$-TS$" term is less than 0.5 meV/atom. For nonmetallic systems, the tetrahedron method with Blöchl corrections[16] is used.

Incremental affine shear strains are imposed on each crystal along experimentally determined common slip systems to obtain the corresponding unrelaxed and relaxed energies and stresses, defined respectively by the conditions, $\epsilon_{ij}=0$ except $s \equiv x/d_0$ with d_0 being the interplanar separation and x taken along the Burgers vector, and $\sigma_{ij}=0$ except for the resolved shear stress. For $\alpha-,\beta-Si_3N_4$, the common slip systems are unknown experimentally. We therefore calculate six systems for each phase, and take the one that has the lowest ideal shear strength.[17]

In Table I, the equilibrium lattice constants $a_0(c_0)$ obtained from energy minimization, with attention to energy cutoff E_{cut} and $\boldsymbol{k}$-sampling convergence, are compared with experimental results. In Table II, the calculated relaxed and unrelaxed shear moduli G_r, G_u in the specified slip systems are compared with analytical values computed from experimental elastic constants. The resolved moduli are calculated using fine meshes $\Delta s = 0.5\% - 1\%$ along the shear path, whereas coarser meshes $\Delta s = 1\% - 5\%$ are used to interpolate the $\sigma(s)$ curves. Affine stress components are relaxed to within a convergence tolerance 0.05 GPa, and in crystals with internal degrees of freedom, the force on each atom is relaxed to less than 0.01 eV/Å.

The relaxed ideal shear stress σ_m^r normalized by G_r and the shearability s_m^r for different materials are plotted together in Fig. 1(a). For simplicity we display only results in the experimentally determined primary slip system, except for

TABLE I. Equilibrium properties: Calculation vs experiment.

Material	# atoms	Method	# ***k***-points	E_{cut}[eV]	a_0, c_0[Å] Calc.	Expt.	Expt. Elastic const [GPa] C_{13}	C_{33}	C_{11}	C_{12}	C_{44}
C	2	US-LDA	$6\times6\times6$	358.2	3.53	3.567[d]			1079.3	125	578.9[e]
Si	2	US-LDA	$5\times5\times5$	188.2	5.39	5.4238[e]			167	65	80[e]
β-SiC	2	US-LDA	$6\times6\times6$	358.2	4.32	4.36[e]			390	142	256[k]
α-Si_3N_4	28	US-LDA	$4\times4\times4$	434.8	7.70,5.58	7.818,5.591[f]					
β-Si_3N_4	14	US-LDA	$4\times4\times8$	434.8	7.56,2.88	7.595,2.9023[g]	127	574	433	195	108[l]
NaCl	8	US-LDA	$6\times6\times6$	274.1	5.46	5.593[e]			57	11.5	13.3[e]
KBr	8	US-LDA	$6\times6\times6$	207.1	6.36	6.566[e]			43	4.8	5.4[e]
MgO	8	US-LDA	$6\times6\times6$	494.6	4.14	4.2072[e]			306	93	158[e]
CaO	8	US-LDA	$6\times6\times6$	494.6	4.57	4.80[e]			210	67	74[e]
Mo	1	US-GGA	$31\times31\times31$	233.1	3.15	3.144[e]			476	158	111[e]
W	1	US-GGA	$31\times31\times31$	235.2	3.17	3.0213[e]			534	205	163[e]
Fe[a]	1	PAW-GGA	$31\times31\times31$	334.9	2.83	2.8603[h]			243	138	122[e]
Ti[c]	2	PAW-GGA	$27\times27\times17$	278.0	2.93,4.63	2.9457,4.6727[e]	68.3	190.5	176	86.9	50.8[m]
Mg	2	PAW-GGA	$39\times39\times25$	262.6	3.19,5.18	3.2094,5.2103[e]	21.7	66.5	63.5	25.9	18.4[e]
Zn	2	PAW-GGA	$33\times33\times23$	345.9	2.64,5.04	2.6638,4.9431[e]	52	69	178	35	46[e]
TiAl	4	US-GGA	$21\times21\times21$	226.5	3.98,4.08	3.975,4.068[i]	74.8	182	187	74.8	109[i]
Ti_3Al	8	US-GGA	$15\times15\times17$	226.5	5.74,4.65	5.814,4.649[j]	62.6	225.1	183.2	89.0	64.1[j]
Al	6	US-GGA	$18\times25\times11$	161.5	4.04	4.0321[e]			114	62	30.8[e]
Ni[a]	1	US-GGA	$31\times31\times31$	302	3.53	3.5136[e]			262	151	132[e]
Ni[b]	1	US-GGA	$31\times31\times31$	302	3.52						
Ag	1	US-LDA	$31\times31\times31$	225.8	4.02	4.07[e]			132	97	51[e]
Au	1	US-LDA	$43\times43\times43$	224.6	4.06	4.08[e]			202	169	45.3[e]
Cu	6	US-GGA	$12\times17\times7$	292.2	3.64	3.616[e]			176.2	124.9	81.8[e]

[a]Ferromagnetic.
[b]Paramagnetic.
[c]*p*-valence.
[d]Reference 23.
[e]Reference 24.
[f]Reference 27.
[g]Reference 28.
[h]Reference 30.
[i]Reference 31.
[j]Reference 32.
[k]Reference 25.
[l]Reference 29.
[m]Reference 26.

BCC metals where all three slip systems are equally likely,[8,18] in which case we use the one that gives the minimum σ_m^r. For Ni we plot only the FM case. The corresponding unrelaxed results are shown in Fig. 1(b). Note that relaxation has a particularly pronounced effect in ionic ceramics.

From these results we see gaps in the distributions of s_m^r and s_m^u between the metals and the covalent solids. Such gaps also may be seen by comparing results of previous works for elastic shear instability of metals[8,12,18] and covalent solids.[17,19] Moreover, among the metals the noble metals Au, Ag, Cu and the more directionally bonded Al and BCC Mo, W, Fe (FM) are at opposite sides of the distributions. This suggests that directional bonding allows for longer-range shear distortion of the bonds before peak resistance is attained, which one can rationalize by observing that the greater the covalency, the more valence charge will concentrate in non-nuclear-centered regions,[20,21] e.g., bond centers and other high-symmetry interstices, as can be verified by an examination of the charge density isosurface plots (see Fig. 2, and also Supplementary Material[22]). These localized charge pockets would require certain spatial arrangement among them for the total energy to be well-minimized. In contrast, if the valence charge density in the interstices is completely delocalized, then there would be no such constraints and the energy barrier to shear would come mainly from a misfit-volume effect. In FCC Cu and Ag one can see that when the local interstice volumes completely recover their equilibrium values at the intrinsic stacking fault, the energy penalities are very low, despite the "wrong" bond angles.[12] Consequently a rather general interpretation of our results is that, so far as the rearrangement of charge density in response to mechanical deformation is concerned, bond-angle dependence brings about geometric constraints on the atomic configurations above and beyond the volumetric constraints. From the standpoint of energy landscape, the stable attractive basin of the ground state is steeper and wider in the shear direction because many low-energy metastable states are eliminated or greatly elevated by the extra constraints in configurational space.

TABLE II. Shear moduli G_r (relaxed), G_u (unrelaxed), ideal shear strains s_m^r (relaxed), s_m^u (unrelaxed) and stresses σ_m^r (relaxed), σ_m^u (unrelaxed) in common slip systems.

Material	Slip system	Expt. G_r	[GPa] [a] G_u	G/B G_r/B	[GPa] [a] G_u/B	Calc. G_r	[GPa] G_u	Relaxed s_m^r	σ_m^r [GPa]	σ_m^r/G_r	Unrelaxed[b] s_m^u	σ_m^u [GPa]	σ_m^u/G_u
C	$\{111\}\langle 110\rangle$	506.8	511.1	1.14	1.15	514.1	519.2	0.325	113.32	0.220	0.374	146.03	0.281
Si	$\{111\}\langle 110\rangle$	57.9	60.4	0.585	0.610	55.2	58.2	0.275	9.62	0.174	0.262	11.13	0.191
β-SiC	$\{111\}\langle 110\rangle$	149.7	168.0	0.666	0.748	158.2	173.4	0.350	31.74	0.201	0.348	43.12	0.249
α-Si_3N_4	$\{11\bar{2}0\}\langle 0001\rangle$					127.3	128.4	0.259	23.72	0.186	0.295	26.48	0.206
β-Si_3N_4	$\{10\bar{1}0\}\langle 0001\rangle$	108.0	108.0	0.417	0.417	101.0	102.0	0.232	19.00	0.188	0.244	21.00	0.206
NaCl	$\{110\}\langle 1\bar{1}0\rangle$	22.8	22.8	0.855	0.855	29.4	29.4	0.221	3.69	0.126	0.658	25.55	0.869
KBr	$\{110\}\langle 1\bar{1}0\rangle$	19.1	19.1	1.09	1.09	23.2	23.2	0.211	2.62	0.113	0.610	15.41	0.666
MgO	$\{110\}\langle 1\bar{1}0\rangle$	106.5	106.5	0.649	0.649	109.5	109.5	0.270	17.09	0.156	0.629	74.34	0.679
CaO	$\{110\}\langle 1\bar{1}0\rangle$	71.5	71.5	0.624	0.624	101.3	101.3	0.277	16.18	0.160	0.664	72.35	0.714
Mo	$\{110\}\langle \bar{1}11\rangle$	138.7	142.8	0.525	0.541	126.5	134.5	0.190	15.18	0.120	0.192	16.52	0.123
Mo	$\{211\}\langle \bar{1}11\rangle$	138.7	142.8	0.525	0.541	126.8	134.1	0.175	14.84	0.117	0.177	15.99	0.119
Mo	$\{321\}\langle \bar{1}11\rangle$	138.7	142.8	0.525	0.541	126.8	134.2	0.176	14.87	0.117	0.175	15.93	0.119
W	$\{110\}\langle \bar{1}11\rangle$	164.0	164.0	0.521	0.521	153.7	155.3	0.179	17.52	0.114	0.196	17.63	0.113
W	$\{211\}\langle \bar{1}11\rangle$	164.0	164.0	0.521	0.521	154.0	155.8	0.176	17.37	0.113	0.175	17.28	0.111
W	$\{321\}\langle \bar{1}11\rangle$	164.0	164.0	0.521	0.521	153.9	155.7	0.176	17.33	0.113	0.175	17.27	0.111
Fe[c]	$\{110\}\langle \bar{1}11\rangle$	64.8	75.7	0.375	0.438	76.6	80.6	0.178	8.14	0.106	0.234	11.43	0.142
Fe[c]	$\{211\}\langle \bar{1}11\rangle$	64.8	75.7	0.375	0.438	75.6	79.9	0.184	7.51	0.099	0.236	9.95	0.124
Fe[c]	$\{321\}\langle \bar{1}11\rangle$	64.8	75.7	0.375	0.438	75.7	80.0	0.181	7.57	0.100	0.197	9.43	0.118
Ti[e]	$\{1\bar{1}00\}\langle 11\bar{2}0\rangle$	44.6	44.6	0.406	0.406	47.6	47.8	0.099	2.82	0.059	0.144	4.92	0.103
Mg	$\{0001\}\langle 11\bar{2}0\rangle$	18.4	18.4	0.499	0.499	19.2	19.2	0.152	1.84	0.096	0.157	2.04	0.106
Zn	$\{0001\}\langle 11\bar{2}0\rangle$	46.0	46.0	0.708	0.708	36.6	36.6	0.132	2.12	0.058	0.136	2.33	0.064
TiAl	$\{111\}\langle 11\bar{2}\rangle$	58.5	61.6	0.524	0.552	50.0	56.4	0.218	5.54	0.111	0.217	6.25	0.111
Ti_3Al	$\{1\bar{1}00\}\langle 11\bar{2}0\rangle$	47.1	47.1	0.416	0.416	50.0	50.8	0.127	5.51	0.110	0.139	5.79	0.114
Al	$\{111\}\langle 11\bar{2}\rangle$	27.4	27.6	0.345	0.348	25.4	25.4	0.200	2.84	0.110	0.210	3.73	0.147
Ni[c]	$\{111\}\langle 11\bar{2}\rangle$	68.8	81.0	0.366	0.431	60.1	79.6	0.140	5.05	0.084	0.160	6.29	0.079
Ni[d]	$\{111\}\langle 11\bar{2}\rangle$					48.8	60.5	0.169	3.17	0.065	0.162	4.70	0.078
Ag	$\{111\}\langle 11\bar{2}\rangle$	22.4	28.7	0.206	0.264	25.0	32.3	0.145	1.65	0.066	0.156	2.57	0.079
Au	$\{111\}\langle 11\bar{2}\rangle$	20.9	26.1	0.116	0.145	17.9	22.9	0.105	0.85	0.048	0.142	1.42	0.062
Cu	$\{111\}\langle 11\bar{2}\rangle$	33.3	44.4	0.235	0.313	31.0	40.9	0.137	2.16	0.070	0.157	3.45	0.084

[a]Computed analytically from expt. elastic constants of Table I.
[b]Subsidiary stress components are unrelaxed, but internal degrees of freedom are relaxed.
[c]Ferromagnetic.
[d]Paramagnetic.
[e]*p*-valence.

In the relaxed s_m^r, σ_m^r distributions [Fig. 1(a)], ionic ceramics lie midway between directionally-bonded metals and covalent solids, while $\alpha-$ and $\beta-Si_3N_4$, being more ionic than SiC, are also in this range.[17] However in unrelaxed shear, these solids manifest abnormally large ideal shear strains s_m^u and stresses σ_m^u, which are attributed to the bare Coulomb repulsion between like-charge ions as in a simple Madelung sum model. In an atomic environment like a crack tip, the surrounding medium would not allow for either fully relaxed or fully unrelaxed local shear. This implies that ionic materials could be either less or much more brittle than covalent materials, depending on the subsidiary deformation constraints present, a situation that is analogous to the distinction of plane-stress vs plane-strain loading conditions in the fracture of metals.

Another noteworthy feature of Fig. 1 is the approximately universal linear scaling between s_m and σ_m/G across a range of crystal structures, nature of bonding, and slip systems. The original Frenkel mode,[1] containing a single parameter G, is well-known and widely used[3–5,33] in an empirical fashion. It

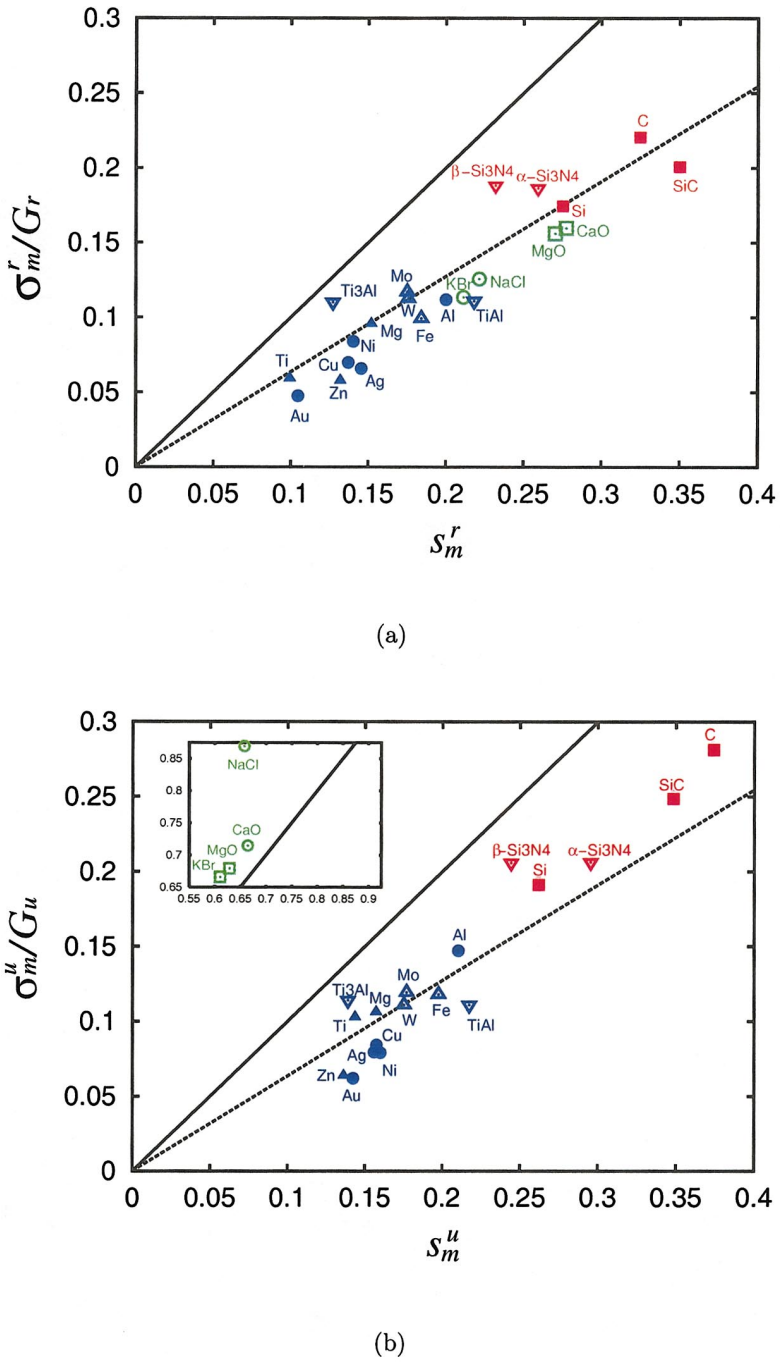

FIG. 1. (Color) DFT calculation results of 22 materials (metallic: blue, ionic: green, covalent: red). (a) Relaxed, and (b) unrelaxed ideal shear stresses (normalized) and shear strains. The solid line indicates a unit slope, while the dashed line corresponds to a slope of $2/\pi$. The ionic solids are far out of range in (b) and are shown in the inset.

has been pointed out, based on physical intuition, that a more realistic description is to treat the peak position of $\sigma(s)$ as an adjustable parameter[6,7] rather than as a fixed value at $b/4d_0$. What we have shown here, on the basis of *ab initio* results, is that a two-parameter representation

$$\sigma = \frac{2Gs_m}{\pi}\sin\left(\frac{\pi s}{2s_m}\right), \quad 0 < s < s_m, \quad \sigma_m = \frac{2Gs_m}{\pi} \qquad (1)$$

with the shear modulus G and the shearability s_m as fundamental materials parameters, provides a satisfactory description of simple metals and ceramics. As can be seen in Fig. 1 the slope of $2/\pi$, implied by our proposed extension of the Frenkel model, Eq. (1), indeed represents the data well. Looking at this correlation in another way, we suggest that the fundamental constitutive behavior for shear deformation can be captured in a master curve in terms of normalized stress $\tilde{\sigma} \equiv \sigma/Gs_m$ and strain $\tilde{s} \equiv s/s_m$, as shown in Fig. 3. In this rescaling all curves have initial unit slope and reach maximum at $\tilde{s}=1$. The behavior labeled as Frenkel (renormalized) reflects a universal shear-softening response, for $s < s_m$.

It is worth emphasizing that this new, "renormalized Frenkel" model is the shear counterpart to the Universal Binding Energy Relation[2] which also has two parameters and has been quantitatively checked against *ab initio* calculations.

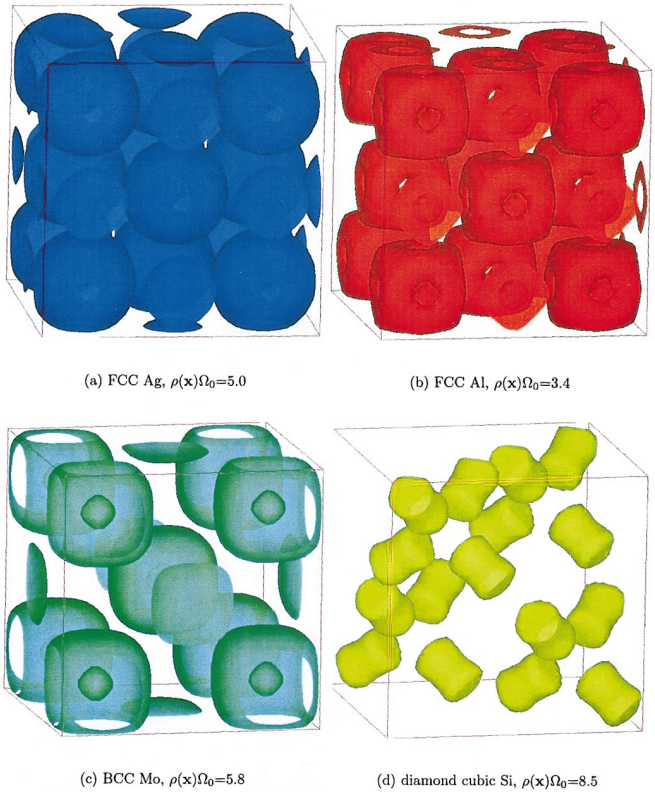

FIG. 2. (Color) Valence charge density $\rho(\mathbf{x})$ isosurface plots of (a) FCC Ag, (b) FCC Al, (c) BCC Mo, (d) diamond cubic Si, at their stress-free states. Ω_0 is the atomic volume.

Taken together they allow materials design and performance criteria to be formulated in which tensile and shear dissipation modes compete.[5,7,33–35] For example, the "brittleness parameter" of Rice[5] that compares the unstable stacking energy γ_{us} to the surface energy γ_s, may be very crudely estimated as

TABLE III. Ideal volumetric tensile strain t_m and stress $-P_m$. B is the bulk modulus computed from DFT.

Material	B[GPa]	t_m	$-P_m$[GPa]	$-P_m/B$
C	433.8	0.623	88.54	0.204
Si	90.16	0.510	15.43	0.171
β-SiC	213.4	0.571	40.59	0.190
α-Si_3N_4	213.9	0.488	41.49	0.194
β-Si_3N_4	226.9	0.594	45.97	0.202
NaCl	28.4	0.527	5.06	0.178
KBr	18.8	0.517	3.08	0.163
MgO	152.0	0.662	31.00	0.204
CaO	104.2	0.670	22.62	0.217
Mo	243.9	0.525	43.17	0.177
W	281.3	0.535	50.17	0.178
Fe[a]	186.5	0.576	28.45	0.153
Ti[b]	107.7	0.618	21.48	0.200
Mg	33.3	0.515	6.01	0.180
Zn	72.5	0.384	9.54	0.132
TiAl	103.2	0.563	19.84	0.192
Ti_3Al	106.9	0.512	20.78	0.194
Al	67.5	0.507	11.15	0.165
Ni[a]	184.0	0.500	29.24	0.159
Ag	114.3	0.514	17.62	0.154
Au	167.9	0.401	23.45	0.140
Cu	130.9	0.478	20.37	0.156

[a]Ferromagnetic.
[b]p-valence.

$$\beta \equiv \frac{\gamma_{us}}{\gamma_s} \propto \frac{G s_m^2}{B t_m^2} = \left(\frac{G}{B}\right) \cdot (s_m^2)/(t_m^2) \tag{2}$$

by scaling arguments. G/B (see Table II) is accessible experimentally and has been used as a performance predictor in

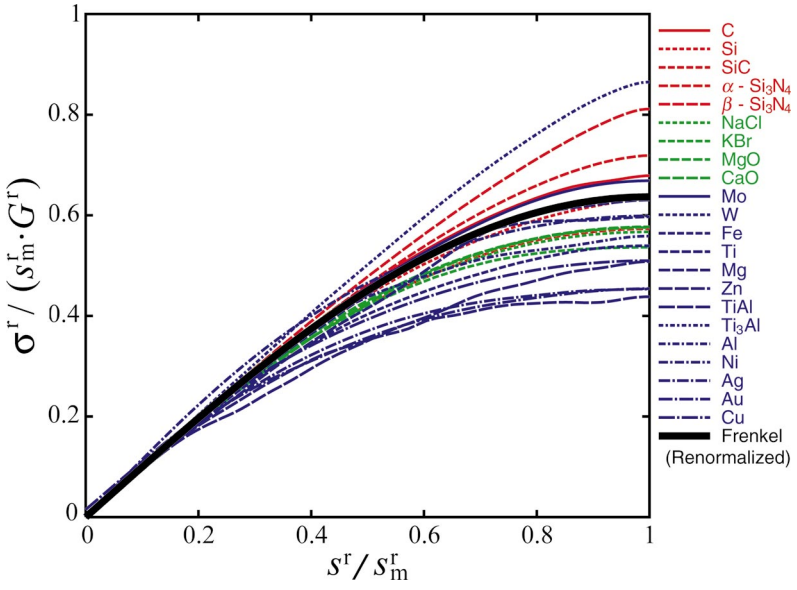

FIG. 3. (Color) Relaxed shear stress-strain curves of 22 materials, rescaled such that all have unit slope initially and reach maximum at 1. The renormalized Frenkel model Eq. (1) is shown for comparison.

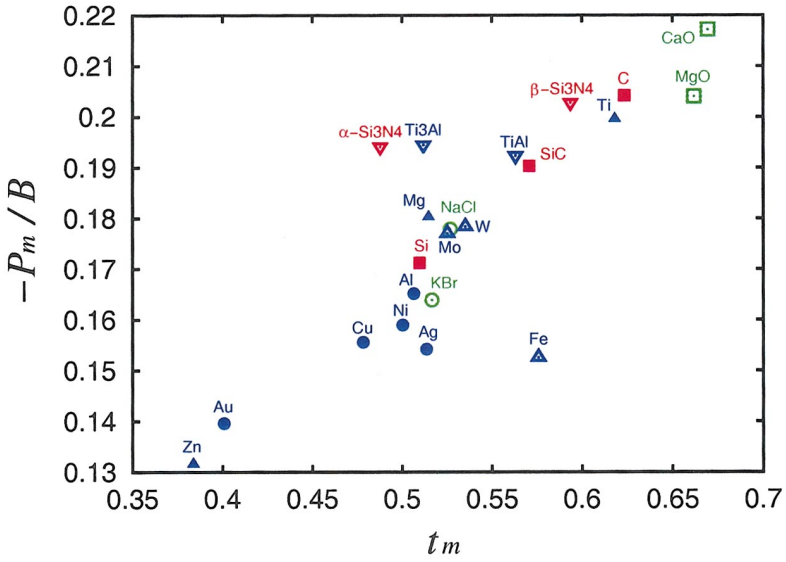

FIG. 4. (Color) Ideal tensile strengths and tensibilities (volumetric) of 22 materials. Note the narrower range of data compared to Fig. 1.

alloy design, for instance to predict the best compromise between ductility and corrosion resistance in stainless steels.[35] But s_m and t_m, while easy to obtain in *ab initio* calculations,[10] are unavailable experimentally and therefore have never been used in a practical manner, despite having been theoretically established to be important.[6,7] Our results, along with other DFT calculations,[8–12,17–19] indicate that a wide gap in β exists between metals and ceramics because G/B and s_m are governed not only by the crystal structure, but also by the nature of bonding (e.g., $s_m^r = 0.105$ in FCC Au vs $s_m^r = 0.200$ in FCC Al) and the loading condition (e.g., $s_m^r = 0.221$ vs $s_m^u = 0.658$ in B1 NaCl). On the other hand, the relative variation of t_m is less sensitive than s_m, and it has no spectral gap (see Table III and Fig. 4). Besides controlling dislocation nucleation[5,7] via Eq. (2), s_m also control dislocation mobility. Based on the model of Foreman *et al.*,[6] it can

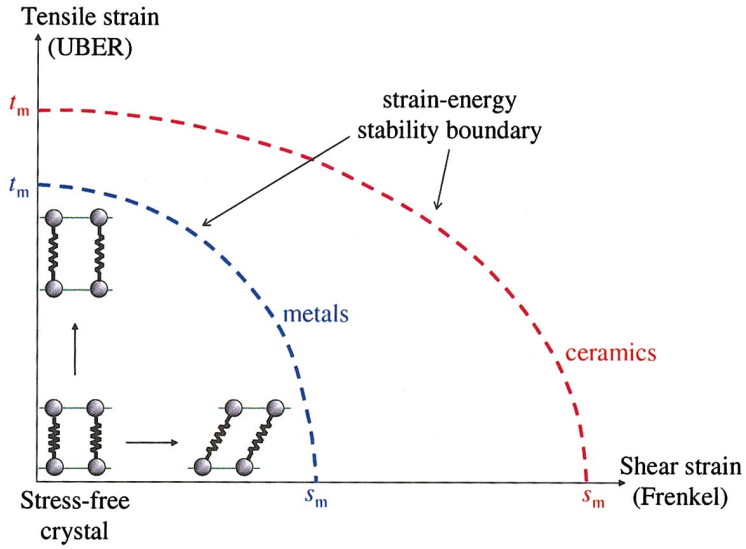

FIG. 5. (Color) Schematic map of material ideal strengths, showing stability boundaries (dashed curves) of the affine strain energy landscapes for metals and ceramics, beyond which bonds break spontaneously in a perfect crystal (Ref. 34). s_m and t_m indicate the maximum stable engineering shear and volumetric tensile strains of a perfect crystal, respectively. Ceramics tend to have larger shearability s_m than metals, with s_m depending not only on the crystal structure (reference value is $b/4d_0$), but also on the nature of bonding (e.g., 0.105 in FCC Au vs 0.200 in FCC Al), and the loading condition (e.g., 0.221 in relaxed vs 0.658 in unrelaxed shear, in NaCl). In contrast, the relative variation of tensibility t_m of solids in more limited (0.38–0.67 in the 22 materials studied). As in the Universal Binding Energy Relation (UBER) (Ref. 2) for tension, a two-parameter model for shear can be established by modifying the empirical formula of Frenkel (Ref. 1). Based on Figs. 1, 3, and 4 and elastic moduli for shear and tension, a simple scaling relation Eq. (2) suggests it is much more difficult to break bonds in ceramic solids in shear than in metals, relative to in tension. Electronic-structure features such as valence charge localization and anisotropy are found to correlate strongly with mechanical-response features during deformation [see Fig. 2 and Supplementary Material (Ref. 22)], such as the shearability.

be shown that increasing the "skewness" $s_m/(b/4d_0)$ of $\sigma(s)$ while keeping G fixed leads to sharply increased Peierls stresses.[3,4]

Our finding is summarized in Fig. 5. We believe there is sufficient basis, in terms of theoretical formulation [1,5–7] and *ab initio* property data,[8–12,17–19] to propose that the shearability s_m of a perfect crystal is an important character of the material. Like the elastic constants, it is a material-specific property that can be determined by first-principles calculations and used in materials design and selection at the macroscopic level. Unlike the elastic constants which pertain to the solid at equilibrium, it reflects quantitatively the electronic and atomic response of the solid at the point of bond breaking.

S.O. thanks M. Kohyama, H. Kitagawa, Y. Koizumi, and M. Nishiwaki and acknowledges support by the Hattori-Houkoukai fellowship. J.L. acknowledges support by Honda R&D Co., Ltd. and the OSU Transportation Research Endowment Program. S.Y. acknowledges support by Honda R&D, AFOSR, DARPA, NSF, and LLNL.

*Electronic address: syip@mit.edu

[1] J. Frenkel, Z. Phys. **37**, 572 (1926).
[2] J. H. Rose, J. R. Smith, and J. Ferrante, Phys. Rev. B **28**, 1835 (1983).
[3] R. Peierls, Proc. Phys. Soc. London **52**, 34 (1940).
[4] F. R. N. Nabarro, Proc. Phys. Soc. London **59**, 256 (1947).
[5] J. R. Rice, J. Mech. Phys. Solids **40**, 239 (1992).
[6] A. J. Foreman, M. A. Jaswon, and J. K. Wood, Proc. Phys. Soc., London, Sect. A **64**, 156 (1951).
[7] G. Xu, A. S. Argon, and M. Ortiz, Philos. Mag. A **72**, 415 (1995).
[8] C. R. Krenn, D. Roundy, J. W. Morris, Jr., and M. L. Cohen, Mater. Sci. Eng., A **319-321**, 111 (2001).
[9] J. W. Morris, Jr., D. M. Clatterbuck, D. C. Chrzan, C. R. Krenn, W. Luo, and M. L. Cohen, Mater. Sci. Forum **426**, 4429 (2003).
[10] M. Černy, J. Pokluda, M. Šob, M. Friák, and P. Šandera, Phys. Rev. B **67**, 035116 (2003).
[11] D. M. Clatterbuck, C. R. Krenn, M. L. Cohen, and J. W. Morris, Jr., Phys. Rev. Lett. **91**, 135501 (2003).
[12] S. Ogata, J. Li, and S. Yip, Science **298**, 807 (2002).
[13] G. Kresse and J. Furthmüller, Phys. Rev. B **54**, 11169 (1996).
[14] P. R. Blöchl, Phys. Rev. B **50**, 17953 (1994).
[15] M. Methfessel and A. T. Paxton, Phys. Rev. B **40**, 3616 (1989).
[16] P. E. Blöchl, O. Jepsen, and O. K. Andersen, Phys. Rev. B **49**, 16223 (1994).
[17] S. Ogata, N. Hirosaki, C. Kocer, and Y. Shibutani, J. Mater. Res. **18**, 1168 (2003).
[18] D. Roundy, C. R. Krenn, M. L. Cohen, and J. W. Morris, Jr., Philos. Mag. A **81**, 1725 (2001).
[19] D. Roundy and M. L. Cohen, Phys. Rev. B **64**, 212103 (2001).
[20] B. Silvi and C. Gatti, J. Phys. Chem. A **104**, 947 (2000).
[21] P. Mori-Sanchez, A. M. Pendas, and V. Luana, J. Am. Chem. Soc. **124**, 14721 (2002).
[22] http://alum.mit.edu/www/liju99/Papers/04/Shearability
[23] J. Donohue, *The Structures of the Elements* (Wiley, New York, 1974).
[24] Landolt-Börnstein III/7a, 7b1, 14a, 29a (Springer-Verlag, Berlin, 1973–1992).
[25] W. R. L. Lambrecht, B. Segall, M. Mathfessel, and M. van Schilfgaarde, Phys. Rev. B **44**, 3685 (1991).
[26] E. S. Fisher and C. J. Renken, Phys. Rev. **135**, A482 (1964).
[27] K. Kato, Z. Inoue, K. Kijima, I. Kawada, H. Tanaka, and T. Yamane, J. Am. Ceram. Soc. **58**, 90 (1975).
[28] R. Grün, Acta Crystallogr., Sect. B: Struct. Crystallogr. Cryst. Chem. **B35**, 800 (1979).
[29] R. Vogelgesang, M. Grimsditch, and J. S. Wallace, Appl. Phys. Lett. **76**, 982 (2000).
[30] M. Acet, H. Zähres, E. F. Wassermann, and W. Pepperhoff, Phys. Rev. B **49**, 6012 (1994).
[31] K. Tanaka, T. Ichitsubo, H. Inui, M. Yamaguchi, and M. Koiwa, Philos. Mag. Lett. **73**, 71 (1996).
[32] K. Tanaka, K. Okamoto, H. Inui, Y. Minonishi, M. Yamaguchi, and M. Koiwa, Philos. Mag. A **73**, 1475 (1996).
[33] J. W. Kysar, J. Mech. Phys. Solids **51**, 795 (2003).
[34] J. Li, K. J. Van Vliet, T. Zhu, S. Yip, and S. Suresh, Nature (London) **418**, 307 (2002).
[35] L. Vitos, P. A. Korzhavyi, and B. Johansson, Nat. Mater. **2**, 25 (2003).